Scientific paper

Nano-structural Changes of C-S-H in Hardened Cement Paste during Drying at 50°C

Yoshimichi Aono[1], Fumiaki Matsushita[1], Sumio Shibata[1] and Yukio Hama[2]

Received 29 June 2007, accepted 20 September 2007

Abstract

Pore structural changes in hardened cement pastes, subjected to drying and wetting/drying cycles, were studied at micrometer and nanometer levels. Characterization techniques included Nuclear Magnetic Resonance (NMR), nitrogen and water vapor adsorption, mercury intrusion porosimetry (MIP) and under-water weighing. Coarsening of pore structure was observed with MIP and increase in the true density of C-S-H was suggested by the result of under-water weighing. Decrease in specific surface area due to drying was observed with nitrogen adsorption, and water vapor adsorption associated with Excess Surface Work (ESW) analysis suggested a development of cohesive structure in C-S-H. NMR confirmed polymerization of silicate anion chains. The drying-induced coarsening of pore structure is probably attributed to polymerization of silicate anion chains and development of cohesive structure in C-S-H.

1. Introduction

Pore structure of hardened cement paste (HCP) is believed as a decisive factor determining properties, such as durability, of cement-based materials. Mercury Intrusion Porosimetry (MIP) and gas adsorption are the widely-applied techniques capable of characterizing the pore structure.

As well known, MIP result of the pore structure of HCP is significantly affected by the prerequisite drying of specimen and coarsening of pore structure depends on the degree of drying. This was attributed to the removal of pore water leaving available space for mercury (Uchikawa *et al*., 1991; Tanaka *et al*., 1994). Oven-dry condition leads to a dehydration and rearrangement of hydration products and results in coarsening of threshold diameter more significantly than D-drying (Moukwa *et al*., 1988; Galle, 2001). The smallest pore diameter depending on the maximum pressure of available MIP equipment is few nanometers and for the total pore volume, including much smaller pores, can be obtained with pycnometric methods such as under-water weighing (Aligizaki, 2006).

Gas adsorption method is a useful technique that has been applied to nano structural analysis of C-S-H by many authors such as Powers (1947), Brunauer (1962), Feldman (1968) and Daimon (1977). Histeresis observed in sorption and desorption of nitrogen or water vapor and specific surface area obtained on the basis of BET method have been mainly discussed, while recently, nano structure of C-S-H was discussed referring to the difference in BET specific surface areas obtained using nitrogen and water vapor (Odler 2003; Jennings and Thomas 2004). Brunauer *et al*. (1979) pointed out that BET specific surface area is significantly affected by the prerequisite drying of HCP. However, because the applicable relative pressure range of the BET method is lower than 0.35, nano structure identification of C-S-H by BET method is limited and information based on entire relative pressure range is not available, which is nevertheless important to identify pore structure and nano structure of C-S-H. Adolphs and Setzer (1996a; 1996b; 1998) proposed Excess Surface Work (ESW) model capable of covering entire relative pressure range while no attempt has been made to analyze HCP subjected to drying with the ESW model.

Silicate anion chains of C-S-H are also affected by drying, while according to the review of Thomas and Jennings (2006), some different opinions have been reported regarding the polymerization of silicate anions. Bentur *et al*. (1979) studied C_3S paste with Trimethylsilylation technique and showed that polymerization of silicate anion developed with drying at younger ages (degree of hydration of 42%) while at later ages (degree of hydration of 68%) the evolution of polymerization was not so active. Parrot and Young (1981) confirmed no polymerization of silicate anions by drying, while Milestone (1980) reported that the polymerization occurred associated with drying regardless of the degree of hydration (ranged from 55 to 86 percent). Hironaga and Sekiguchi (1999) noted that C-S-H changes with drying resulting in a condensation of silicate anion chains.

The coarsening of HCP pore structure due to drying has been mainly discussed in terms of the specimen preparation for MIP and confirmed in many researchers while a claim that MIP can hardly provide a valid pore size distribution was made by Diamond (2000). The coarsening of pore structure is a problem not only of measurement condition but also of durability because the working environment of HCP includes such dry and

[1]Sumitomo Metal Mining Siporex, Co. Ltd., Tokyo, Japan.
E-mail:Yoshimichi_Aono@ni.smm.co.jp
[2]Muroran Institute of Technology, Muroran, Japan.

elevated temperature conditions in summer. Exploring the reason of the drying impact is thus very important if we consider that the strength and durability such as frost resistance are normally discussed and designed on the basis of MIP results.

The drying of HCP poses an impact not only on the pore structure but also on the specific surface area and polymerization of silicate anions while systematic studies of this issue are very few. In this paper, we focused on changes in pore structure of HCP and nano-structure of C-S-H, the major constituent of HCP, using MIP, under-water-weighing method, gas adsorption and NMR. Analysis of the gas adsorption was performed with the ESW model which covers wider relative pressure ranges than that of BET method. Thermogravimetry was also carried out to examine the effect of degree of hydration.

2. Experiments

2.1 Specimen preparation

Specimens of hardened cement pastes were prepared using ordinary portland cement with a water-cement ratio of 0.35. The chemical composition of the cement is shown in **Table 1**. Curing conditions are listed in **Table 2**. Mixing was performed with a mortar mixer and the slurry was placed to a height of 6 cm in a steel mold of 8 x 4 x 16 cm. After one-day sealed curing and subsequent de-molding, specimens were shaped into 4 x 4 x 16 cm by removing top 2 cm to avoid possible bleeding effects and subjected to under-water curing at 20°C for four weeks. Curing of specimen 35W20 was prolonged another four weeks, while 35D50 was subjected to oven-drying at 50°C for four weeks. To imitate changes in the working environment of HCP as a factor affecting its pre structure, 35DW30 and 35DW50 were subjected to four wetting-drying cycles of 5-day drying at 30 and 50°C, and subsequent 2-day of water immersion.

After curing, specimens were crushed into particles with a diameter of approx. 2.5 to 5 mm, treated with acetone to suspend hydration and kept under the D-dry, carbonation-free, condition until the test. Specimens for nitrogen and water vapor sorption isotherms and for NMR were finely ground in a mortar.

2.2 Test method

Specimens were first D-dried, ground in a mortar and subjected to thermogravimetry (Bruker AXS TG-DTA 2010SA) at a heating rate of 2°C under nitrogen gas flow. Operation temperature was from room temperature to 1000°C. Dehydration of $Ca(OH)_2$ around 500°C, LOI(CH), carbon dioxide release around 600 to 800°C, LOI(CC) and dehydration of cement hydrates other than $Ca(OH)_2$, LOI(Hyd) were determined using equations (1), (2) and (3) respectively.

$$\mathrm{LOI(CH)(\%)} = \frac{\mathrm{Ca(OH)_2\ mass\ loss\ around\ 500\ °C}}{\mathrm{sample\ mass\ at\ 1000\ °C}} \times 100 \quad (1)$$

Table 1 Characters of the ordinary portland cement.

Items	Characters
Density (3.16g/cm^3)	3.16
Specific surface area (cm^2/g)	3250
28-day compressive strength (N/mm^2)	63.8
MgO(%)	1.9
SO_3(%)	1.8
SiO_2(%)	21.5
Al_2O_3(%)	5.5
Fe_2O_3(%)	2.9
CaO(%)	64.3
LOI(%)	0.64

Table 2 Curing conditions.

Sample	W/C	Water curing	Environmental change condition
35W20	0.35	2 weeks at 20°C	Water curing for 4 weeks at 20°C
35DW30			[Air curing for 5 days at 30 °C ↔ water curing 2 days at 20 °C] × 4 cycles
35DW50			[Air curing for 5 days at 50 °C ↔ water curing 2 days at 20 °C] × 4 cycles
35D50			Air curing for 4 weeks at 50 °C

$$\mathrm{LOI(CC)(\%)} = \frac{\mathrm{CaCO_3\ mass\ loss\ from\ 600\ to\ 800\ °C}}{\mathrm{sample\ mass\ at\ 1000\ °C}} \times 100 \quad (2)$$

$$\mathrm{LOI(Hyd)(\%)} = \mathrm{(mass\ loss\ from\ 105\ to\ 1000\ °C) - LOI(CH) - LOI(CC)} \quad (3)$$

Pore size distribution was determined with MIP using specimens that were ground and graded with a diameter of 1.0 to 2.0 mm. Micromeritics Auto-Pore 9200 was used at the maximum pressure of 150 MPa and the results were analyzed using Washburn's formula (1921).

Under-water weighing was performed with crushed and D-died specimen, which was first immersed in water and subjected to 4-hour vacuum deaeration. After determining the masses in water, in the saturated surface-dry condition and after oven-drying at 105°C for 24 hours, bulk density (the inverse of specific volume), true density (the inverse of specific true volume), total porosity and total pore volume were calculated using the following equations (4), (5) and (6).

$$\rho_{ap} = \frac{1}{v_{ap}} = \frac{m_d \rho_w}{m_s - m_w} \quad (4)$$

$$\rho_{tr} = \frac{1}{v_{tr}} = \frac{m_d \rho_w}{m_d - m_w} \quad (5)$$

$$V_{total} = v_{ap} - v_{tr} \tag{6}$$

where ρ_{ap} (g/cm^3): apparent density, v_{ap} (cm^3/g): apparent specific volume, ρ_w (g/cm^3): density of water, m_d (g): mass of specimen after oven drying at 105°C, m_s (g): mass of saturated surface-dried specimen, m_w (g): mass of saturated specimen immersed in water, ρ_{tr} (g/cm^3): true density, v_{tr} (cm^3/g): true specific volume and V_{total} (cm^3/g): total pore volume.

Nitrogen sorption isotherm was determined after degassing for two hours using Quantachrome NOVA1000. Specific surface area was calculated using BET (Brunauer-Emmett-Teller) method (Brunauer *et al*., 1938) and pore size distribution was obtained according to DH (Dollimore-Heal) method (Dollimore and Heal, 1964). A nitrogen molecular area of 0.162 nm^2 was adopted for the specific surface area calculation (McClellan and Harnsberger, 1967).

Water vapor sorption isotherm was determined at 25°C after a prerequisite drying in vacuum at 20°C for 24 hours using Bell Japan's BELSORP P18-Plus. Analysis was performed not only with BET method but also with the ESW model proposed by Adolphs and Setzer (1996a; 1996b; 1998). ESW Φ is defined with the following formulas,

$$\Phi = n_{ads}\Delta\mu \tag{7}$$

$$\ln|\Delta\mu| = -\frac{1}{n_{mono}} \cdot n_{ads} + \ln|\Delta\mu_0| \tag{8}$$

where n_{ads} is the amount adsorbed and $\Delta\mu$ is a change in chemical potential defined as $\Delta\mu=RT\ln(p/p_s)$. **Figure 1** shows the plots of Eqs. (7) and (8) represented with the ESW model, where a minimum is shown in **Fig. 1 (a)**. ESW has a physical content of the adsorption energy of molecule per unit mass of adsobent and shows a minimum at monolayer adsorption n_{mono}. A line with a negative gradient is shown in **Fig. 1(b)** where the inverse of the gradient gives n_{mono}. Specific surface area can be obtained multiplying n_{mono} by the molecular area of gases. Moreover with **Fig. 1(b)**, changes in the specific surface area with an increase in n_{ads}, i.e. with changes in adsorption state at multilayer adsorption, can be discussed (Adolphs and Setzer, 1998). A water molecular area of 0.114 nm^2 was adopted for the specific surface area calculation (Brunauer and Greenberg, 1962).

NMR measurement was performed according to ^{29}Si-NMR (MAS) method at a frequency of 79.45 MHz, acquisition time of 10 seconds and number of points of 5000 using Bruker Biospin AVNCE400. The obtained spectrum was subjected to deconvolution using Gaussian/Lorenzian scheme of the dedicated software Bruker WinFit. When ^{29}Si nuclei are subjected to NMR, silicate anions (SiO_4^{4-}) in a calcium silicate compound show Q_0 to Q_4 peaks in the spectrum representing their chain structures. In C-S-H, the major constituent of HCP, Q_1 (chain end) and Q_2 (within chain) are the major chain configuration and neither Q_3 (branching chain) nor Q_4 (networked chain) can be observed (Grimmer 1994). Coordination of silicate anion chains with the layered structure of $Ca(OH)_2$ was reported by Birchall (1984). Klur *et al* (1998) separated Q_2 peaks into three types by ligand ions: Q_{2p} (H^+ coordination), Q_{2i} (interlayer Ca^{2+} coordination) and Q_{2Ca} (CaO lyaer coordination), but the separation is normally difficult because Q_{2i} peak is not intensive and overlapping with Q_{2Ca}. **Fig. 2** shows the schematic silicate anion structure with coordination of Q_1, Q_{2Ca} and Q_{2p}.

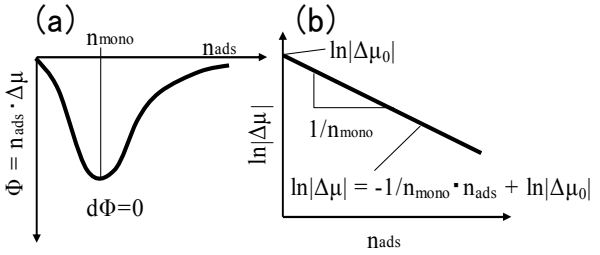

Fig. 1 Plots of ESW model (a): ESW (Φ) vs. amount adsorbed (b): plots of logarithm method.

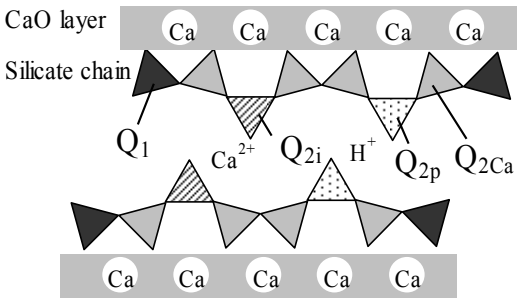

Q_1; -79ppm Q_{2p}; -82ppm Q_{2i}; -84ppm Q_{2Ca}; -85ppm

Fig. 2 Schematic structure of C-S-H and assignment of Q_n (redrawn of Klur *et al*., 1998).

Because silicate anion chain of C-S-H resulting from cement hydration is a straight chain, the geometrical relation gives averaged polymerization degree N using eq. (9).

$$N = 2 \times Q_{2total}/Q_1 + 2 \tag{9}$$

where $Q_{2total}=Q_{2p}+Q_{2Ca}$ is assumed. According to the method of Parry-Jones *et al*. (1989), peak intensity ratio I_{Q0} of Q_0 originated from unreacted cement is determined and the degree of cement hydration a was obtained using eq. (10).

$$\alpha = 1 - I_{Q0} \tag{10}$$

3. Results and discussions

3.1 TG

TG curves are shown in **Fig. 3** where specimens exhibit

almost similar mass loss rate except for that of 35D50 that becomes smaller around 200 to 500°C. Mass loss rate of the specimens determined with eqs. (1), (2) and (3) is shown in **Fig. 4**. Comparison of LOI(CC) suggests that all the specimens were almost equally carbonated as also shown in **Fig. 3**. LOI(CH) of specimens subjected to drying or wetting/drying are larger than that of the control specimen suggesting that the hydration was at least not interrupted by drying. LOI(Hyd) of specimen subjected to drying, 35D50, was approx. one percent smaller than that of the others, which may be attributed to the low mass loss rate around 200 to 400 °C as shown in **Fig. 3**. According to Uchikawa *et al*. (1980), ettringite has the dehydration TG peak at 120 °C and partially decomposed by D-drying, and monosulfate shows three dehydration TG peaks around 50 to 120 °C, 120 to 200 °C and 230 to 300 °C. Hence the decrease in LOI(Hyd) of 35D50 may not at least be attributed to the decomposition of ettringite and have possibilities of dehydration of C-S-H or decomposition of monosulfate corresponding to the third dehydration peak. This will be discussed in terms of the degree of hydration of HCP and dehydration of C-S-H referring to the results of ^{29}Si-NMR.

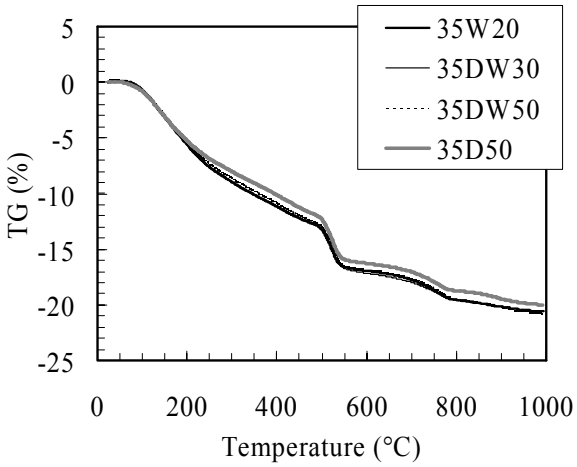

Fig. 3 TG curves.

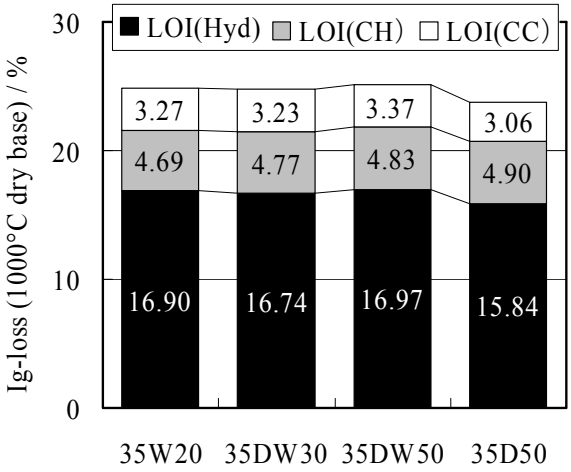

Fig. 4 Comparison of LOI(Hyd), LOI(CH) and LOI(CC).

3.2 MIP

Pore size distributions obtained with MIP are shown in **Fig. 5**. No significant difference was found between 35D30 and control specimen. Both in 35DW50 and 35D50, cumulative pore volume with a diameter greater than 8 nm, the measurable lower limit of MIP, increased as shown in **Fig. 5(a)**. Partial pore volumes with a diameter from 20 to 100 nm and from 20 to 500 nm increased in 35DW50 and 35D50 respectively as shown in **Fig. 5(b)**.

Drying-induced pore size distribution shift to a coarser region was discussed by Galle (2001). Extent of the shift was in an order of 105°C oven-drying, 60°C oven-drying, vacuum-drying (10 Pa, equivalent to D-drying) and freeze-drying. MIP specimens in this study were first subjected to wetting/drying cycle at 50°C and then D-dried, hence the temperature history could contribute to the coarsening of pore size distribution.

Duration of 50°C oven-drying was probably the major factor controlling the degree of coarsening because the above coarsening was more significant in 35D50 (drying only) than in 35DW50 (drying and wetting). Further study of the drying-induced pore size distribution shift is needed under variable drying temperature and processing time, but in this study, this effect is considered as a given difference in the degree of drying.

3.3 Under-water weighing

Pore structure parameters calculated using Eqs (4)-(6) are shown in **Table 3**. True density of HCP showed an increase suggesting a possibility of increase in true density of C-S-H that is the major constituent of HCP. Drying-induced changes in volume of pore and solid part of HCP are compared in **Fig. 6**. Pore volumes of HCP

Table 3 Results of under-water weighing using Equations (1) to (3).

Specimen	Apparent density ρ_{ap} (g/cm^3)	Apparent specific volume v_{ap} (cm^3/g)	True density ρ_{tr} (g/cm^3)	True specific volume v_{tr} (cm^3/g)	Total pore volume V_{total} (cm^3/g)
35W20	1.72	0.581	2.34	0.427	0.154
35D30	1.71	0.583	2.41	0.415	0.168
35DW50	1.76	0.568	2.50	0.400	0.169
35D50	1.79	0.560	2.56	0.390	0.169

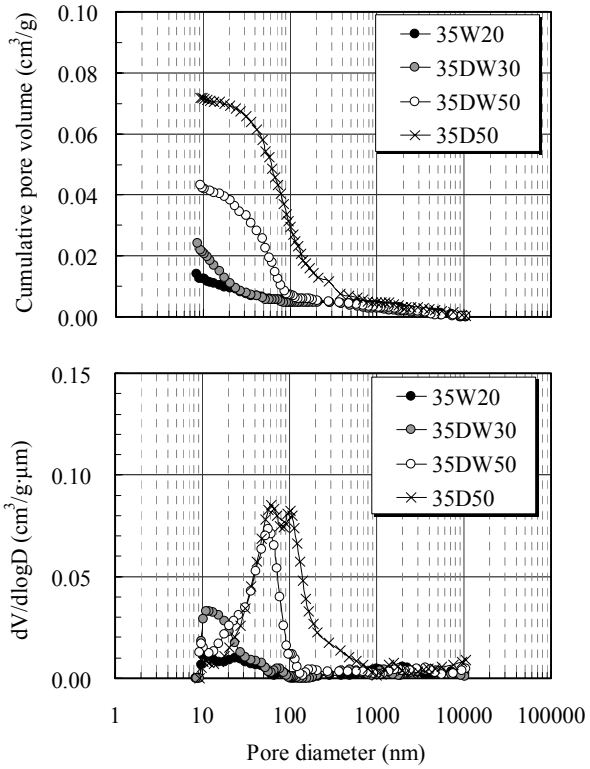

Fig. 5 Pore size distributions measured with MIP.

comprise the true specific volume v_{tr} that is the solid part of C-S-H, mercury-accessible volume with a pore diameter greater than 8 nm V_{Hg} and the remaining pore volume as expressed in Eq. (11),

$$v_{ap} = (V_{total} - V_{Hg}) + V_{Hg} + v_{tr} \tag{11}$$

where v_{ap} (cm^3/g): apparent specific volume in Eq. (4), V_{total} (cm^3/g): total pore volume in Eq. (6), V_{Hg} (cm^3/g): mercury-accessible volume with a pore diameter greater than 8 nm and v_{tr} (cm^3/g): true specific volume in Eq. (5). With an increase in degree of drying, v_{tr} decreases and V_{Hg} increases, and V_{total}- V_{Hg} decreases accordingly. This implies that the solid part of HCP shrunk with a development of cohesion and increase in large pores with a diameter greater than 8 nm. As Galle (2001) noted, V_{total} is overestimated when 105°C oven-drying is adopted as a standard dry mass compared to those using vacuum-drying and 60°C oven-drying. This is because the water content differs according to drying conditions. In this study, the standard dry mass was determined using 105°C oven-drying for all the specimens, therefore the change in V_{total} was most probably caused by drying or drying-wetting at 50°C and not by the operation of obtaining the standard dry mass.

3.4 Nitrogen adsorption

Nitrogen sorption isotherms for HCP are shown in **Fig. 7** where specific surface areas determined with BET method are also shown. Compared to the non-treated specimen (35W20), amount of nitrogen adsorption, hysteresis and BET (N_2) specific surface area generally decreased according to the drying condition, i.e. in an order of 50°C drying and wetting (35DW50) and 50°C drying (35D50). The decrease of hysteresis implies changes in pore structure of HCP or nano structure of C-S-H.

Decrease in BET (N_2) surface area due to drying may be explained by the Colloid Model proposed by Jennings (2000), where unit particles, the basic building blocks with a diameter approx. 1 nm, are forming a colloidal particle, a higher-order structure called Globule. C-S-H can be classified in LD C-S-H and HD C-S-H according to the cohesive structure of Globules, where LD C-S-H allows nitrogen gas to enter while HD C-S-H does not. When C-S-H is subjected to drying, LD C-S-H becomes more cohesive and prevents nitrogen gas molecules from entering in the structure resulting in the decrease in BET (N_2)

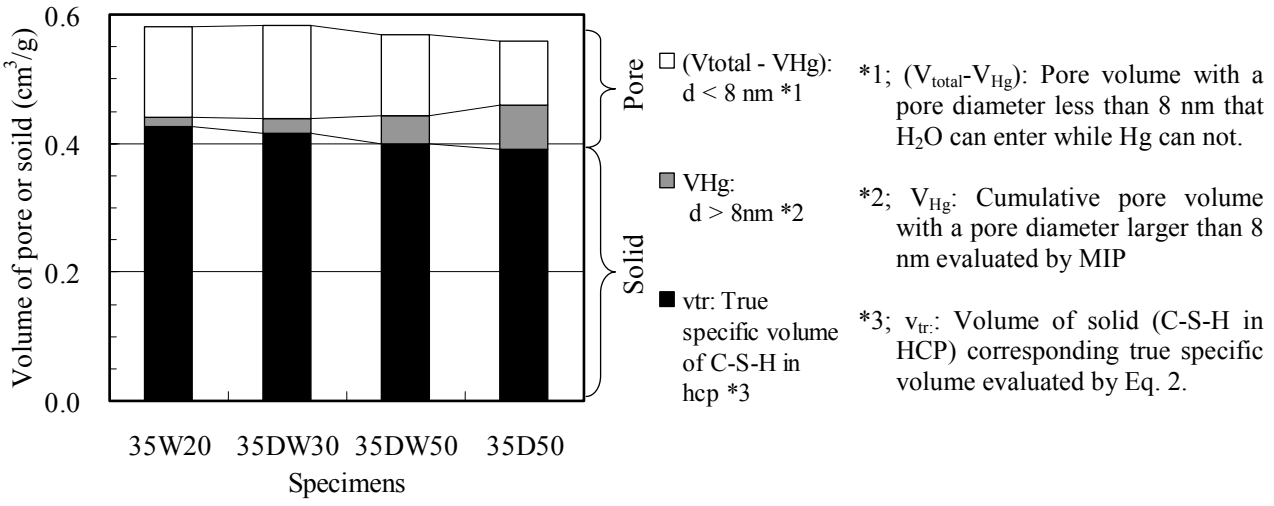

Fig. 6 Comparison of specific volume of pore and solid in HCP.

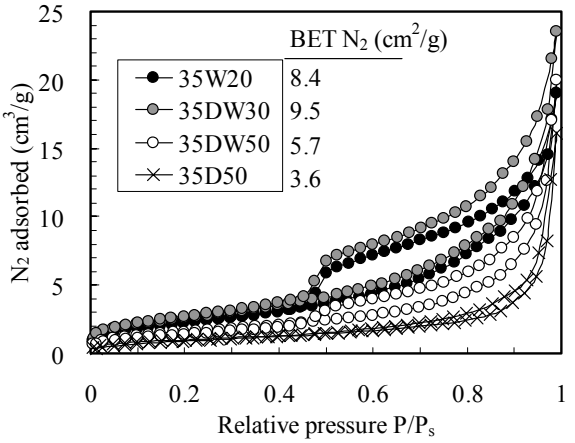

Fig. 7 N_2 sorption isotherm of HCP.

specific surface area. This implies the drying-induced densification of C-S-H and corresponds to the increase in the true density of HCP as shown in **Table 2**.

Pore size distributions for HCP calculated with DH method (Dollimore and Heal, 1964) are shown in **Fig. 8**. Compared to the non-treated specimen (35W20), total pore volumes measured with nitrogen decrease according to the drying condition, i.e. in an order of 50°C drying and wetting (35DW50) and 50°C drying (35D50). A marked decrease in pore volume can be found at a pore volume with a pore diameter around 7 nm showing good agreement with the decrease in pore volume with a diameter less than 8 nm (V_{total}- V_{Hg}) measured with under-water weighing as shown in **Fig. 7**.

3.5 Water vapor adsorption

Water vapor sorption isotherms of specimens are shown in **Fig. 9**. Compared to the non-treated specimen (35W20), amount of adsorption and hysteresis decrease according to the drying condition, i.e. in an order of 30 and 50°C drying and wetting (35DW30, 35DW50) and 50°C drying (35D50). Also BET (H_2O) specific surface areas decrease with an extent of drying. Applicable relative pressure range of BET method is limited between 0.05 and 0.35 and the resulting specific surface area is based on the monolayer adsorption while the difference in water vapor sorption isotherms as shown in **Fig. 9** occur at higher relative pressure range implying that the drying-induced structural changes are represented at multilayer adsorption states.

This assumption were verified with ESW model proposed by Adolphs and Setzer (1996; 1998) using Eqs (7) and (8). The results are shown in **Fig. 10** where the ESW minima at the monolayer adsorption show positive increase due to drying implying the lowering of adsorption energy at the monolayer adsorption as shown in **Fig. 10(a)**. It is also shown in **Fig. 10(b)** that a knick point is present at the monolayer adsorption state and the gradient, corresponding to a specific surface area, increases with an intensity of drying, implying the lowering of the

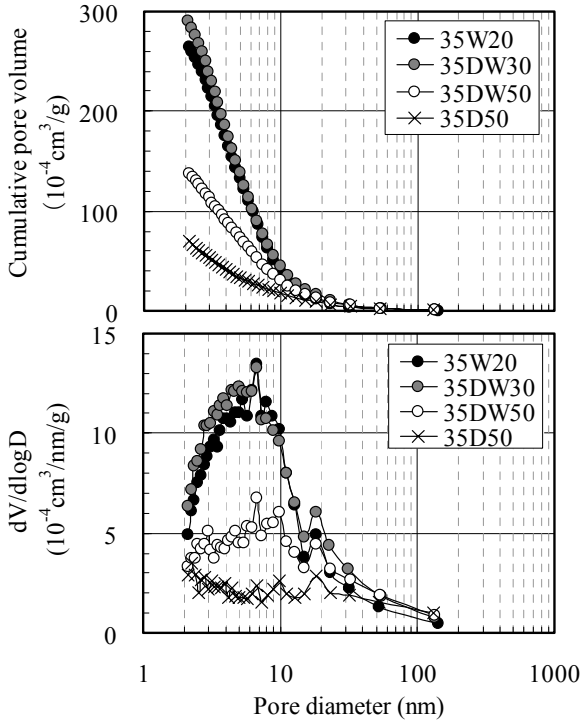

Fig. 8 Pore size distribution of HCP with N_2 by DH method.

specific surface area of C-S-H at multilayer adsorption states.

Specific surface areas at monolayer and multilayer adsorption states can be calculated using Eq. (8) and the results of analysis are shown in **Fig. 11**. Results of specific surface area determined in this study are shown in **Table 4** where BET-H_2O and ESW S1-H_2O show good agreement.

Specific surface areas with BET-N_2 and those using water vapor are compared in **Fig. 12** where BET-N_2 shows a single digit smaller specific surface area than those using water vapor. Drying-induced changes in specific surface areas with water vapor are almost equal

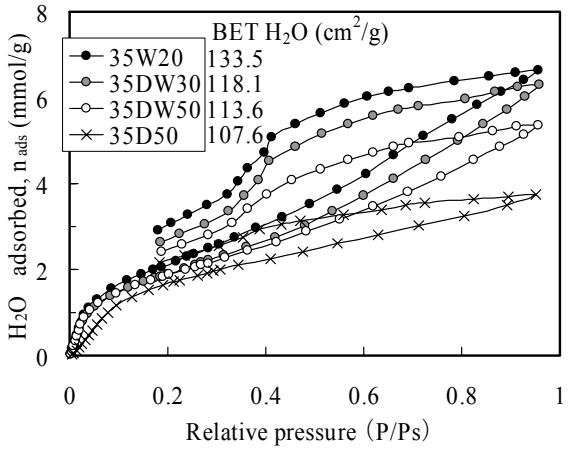

Fig. 9 H_2O sorption isotherm of HCP.

to those with BET-H_2O and ESW S1-H_2O while that of ESW S2-H_2O is much larger. Jennings (2000) attributed the drying-induced changes in specific surface areas of BET-H_2O to an aggregation of LD C-S-H while the result of ESW S2-H_2O further suggests that the specific surface

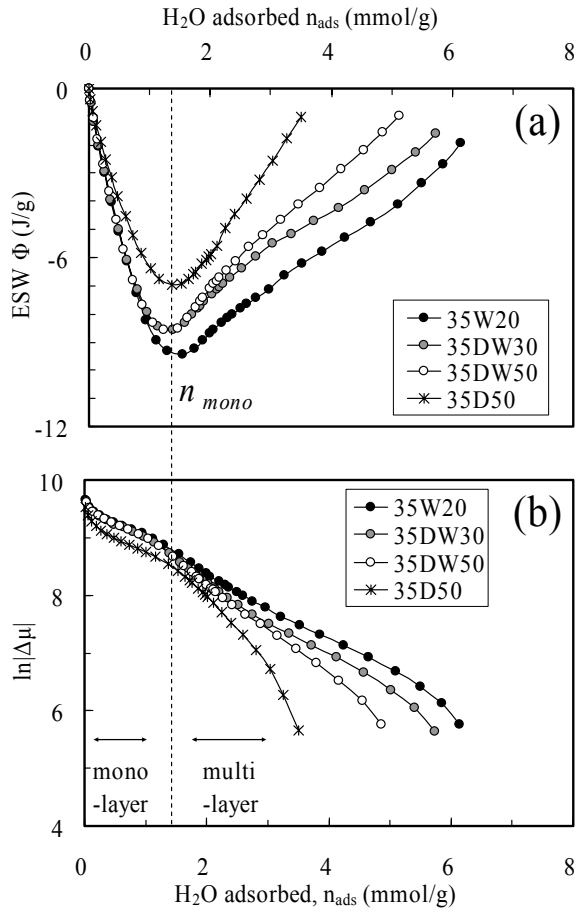

Fig. 10 ESW analysis of water vapor adsorption isotherms of HCP (a): ESW (Φ) vs. amount adsorbed (b): plots of logarithm method.

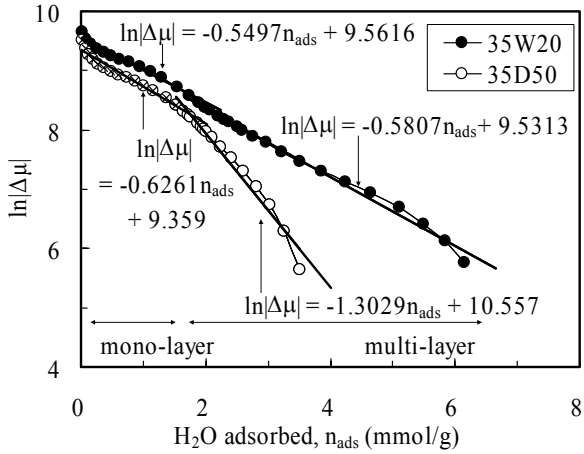

Fig.11 ESW analysis of surface areas at mono- and multi-layer adsorption state.

Table 4 Specific surface area.

Specimen	Nitrogen adsorption (m^2/g)	Water vapor adsorption (m^2/g)		
	BET	BET	ESW	
	BET N_2	BET H_2O	S1 H_2O	S2 H_2O
35W20	8.4	133.5	124.8	118.2
35DW30	9.5	118.1	112.5	105.8
35DW50	5.7	113.6	117.7	88.0
35D50	3.6	107.6	109.6	52.7

ESW S1 H2O; mono-layer
ESW S2 H2O; multi-layer

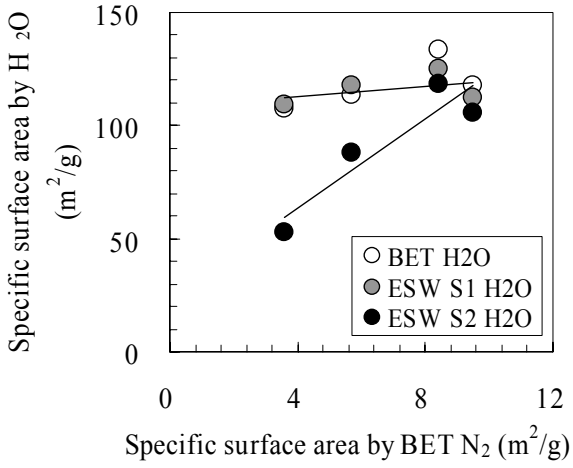

Fig. 12 Comparison of specific surface areas by Nitrogen adsorption (BET N_2) and water vapor adsorption (BET H_2O, ESW S1 H_2O and ESW S2 H_2O).

area at multilayer adsorption decreases significantly.

Conventional knowledge showed that specific surface areas of HCP with BET-H_2O is almost constant regardless of water-cement ratio, age and prerequisite drying condition and is always greater than that with BET-N_2 (Feldmann 1968; Odler 2003). This is a consequence of calculating the specific surface areas using monolayer capacity. Because water molecules can access to the nano space of HCP, ESW analysis of changes in specific surface area at multilayer adsorption is likely to figure out the aggregation of C-S-H. The result of ESW analysis may also attribute the coarsening of pore structure observed with MIP to the drying-induced aggregation of C-S-H.

3.6 Nuclear Magnetic Resonance

NMR output was analyzed following the chemical shifts shown by Klur *et al*. and Q_2 was separated into Q_{2p} and Q_{2Ca}. As shown in **Fig. 13**, increase in Q_{2Ca} by drying can

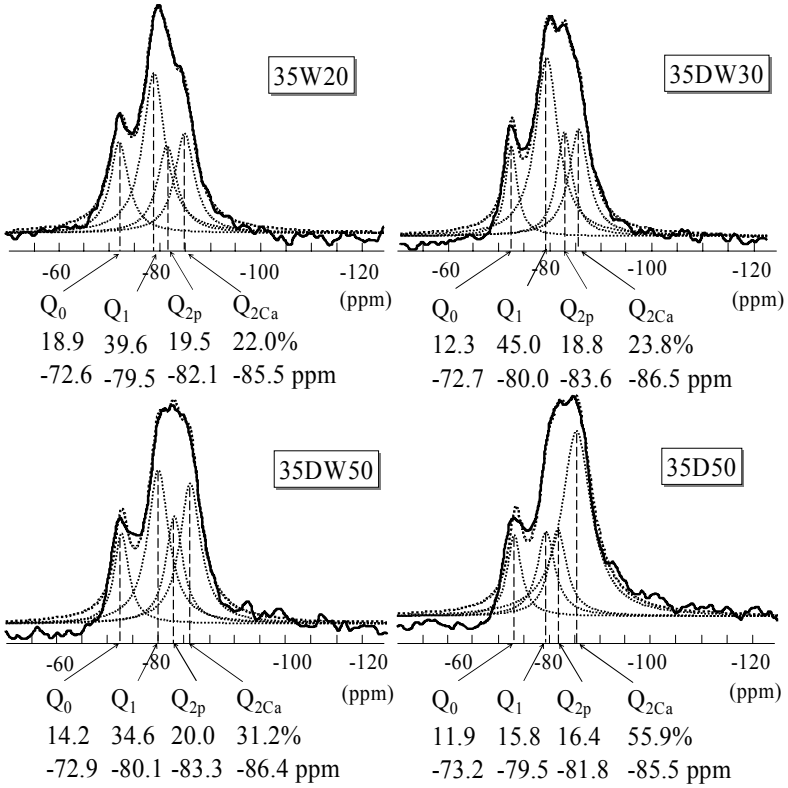

Fig. 13 ^{29}Si NMR MAS spectra of C-S-H in HCP.

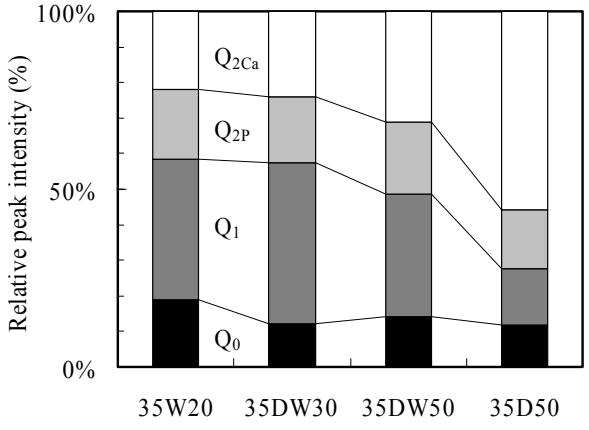

Fig. 14 Comparison of relative peak intensity of C-S-H in HCP by ^{29}Si NMR MAS.

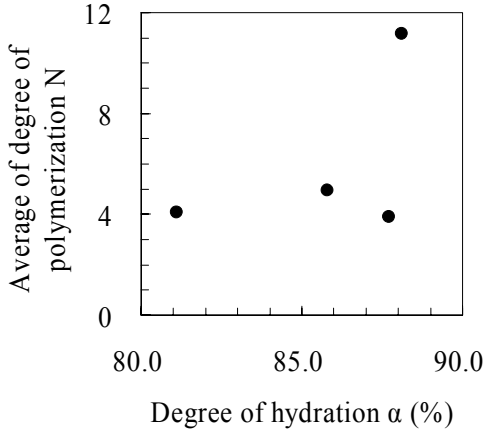

Fig. 15 Average of degree of hydration N vs. degree of hydration α.

be observed. Drying-induced changes in peak intensity are compared in **Fig. 14** where Q_1 decreases and Q_{2Ca} increases. The average of the degree of silicate anion polymerization and the degree of hydration calculated with Eqs. (9) and (10) are shown in **Table 5**. As shown in **Fig. 15**, the polymerization of silicate anion does not depend on the degree of cement hydration. This is supported by the report of Brough *et al*. (1994) showing that Q_2 increased with decrease in Q_1 after the fully hydrated ages of more than 100 days. Decrease in LOI(Hyd) of 35D50 as shown in TG results of **Figs. 3** and **4** suggests that a dehydration condensation of C-S-H may be advancing. This implies that polymerization of silicate anions coordinated with CaO layer developed when C-S-H was subjected to drying.

3.7 Pore structure and nano-structural changes due to drying

Above results show that pore structural changes in HCP during drying can be attributed mainly to changes in C-S-H structure at nano levels. Relationship between specific surface area with BET-N_2 and degree of polym-

Table 5 Degree of polymerization *N* and degree of hydration α.

Specimen	Degree of polimerization *N*	Degree of hydrationα α
35W20	4.1	81.1
35DW30	3.9	87.7
35DW50	5.0	85.8
35D50	11.2	88.1

N; Eq.(9), α; Eq.(10)

erization of silicate anions (Q_{2total}) is shown in **Fig. 16**. With an increase in Q_{2total}, BET-N_2 decreases significantly implying that the drying-induced changes in specific surface area with BET-N_2 is associated with polymerization of silicate anions, which was also noted by Jennings (2000; 2004).

Relationship between specific surface area with BET-H_2O, ESW S1-H_2O and ESW S2-H_2O, and Q_{2total} is shown in **Fig. 17**. Change in specific surface area at monolayer adsorption state (BET-H_2O and ESW S1-H_2O) with an increase in Q_{2total} is slight while at multilayer adsorption (ESW S2-H_2O), it decreases significantly. This also implies an aggregation of C-S-H as seen in BET-N_2.

Relationships of pore volumes (V_{total} and V_{Hg}) and specific volume of solid (v_{tr}) with respect to Q_{2total} are shown in **Fig. 18**, where V_{total} shows no or slight increase but V_{Hg} tends to increase. This leads to a conclusion that the drying-induced pore coarsening was caused by the development of polymerization of silicate anion chains resulting in a formation of new pore spaces.

4. Conclusions

When HCP was subject to drying at 50 °C, pore structure and C-S-H nano structure changed in the following manner:

(1) Pore volume with a diameter greater than 8 nm increased as measured by MIP.

(2) True density measured by the under-water weighing increased and pore volume with a diameter smaller than 8 nm decreased while the total pore volume remained unchanged.

(3) Specific surface area measured with BET-N_2 decreased significantly.

(4) Specific surface area measured with BET-H_2O showed good agreement with that obtained by ESW model at monolayer adsorption state (ESW S1-H_2O) and decreased slightly by drying, while that at multilayer adsorption state (ESW S2-H_2O) decreased significantly in the same manner as in BET-N_2.

(5) Polymerization of silicate anion chain was induced by drying as observed in ^{29}Si-NMR and no correlations between silicate anion polymerization and degree of hydration of HCP were recognized.

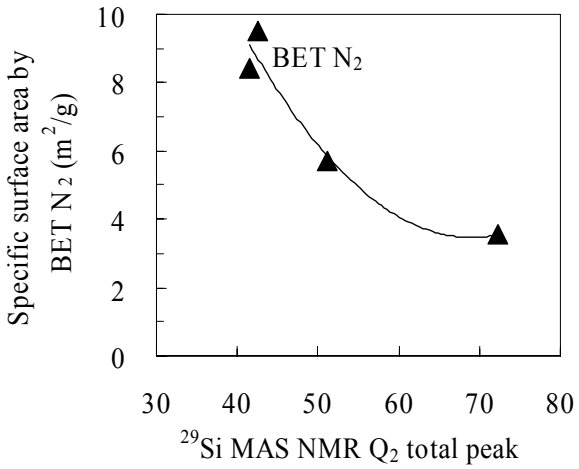

Fig. 16 Relationship between specific surface area of BET N_2 and Q_{2total} by NMR.

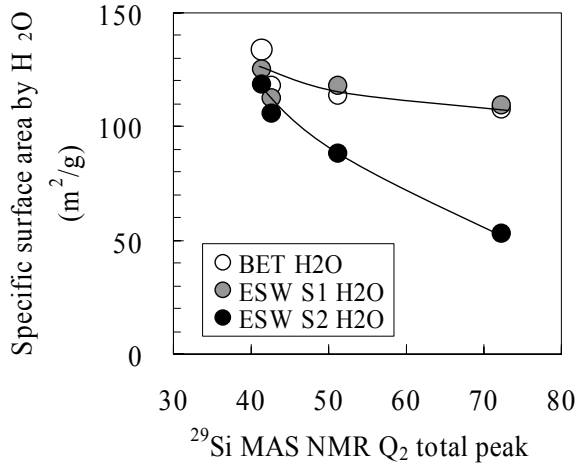

Fig. 17 Relationship between specific surface areas at mono- and multi-layer adsorption state by ESW (H_2O) and Q_{2total} by NMR.

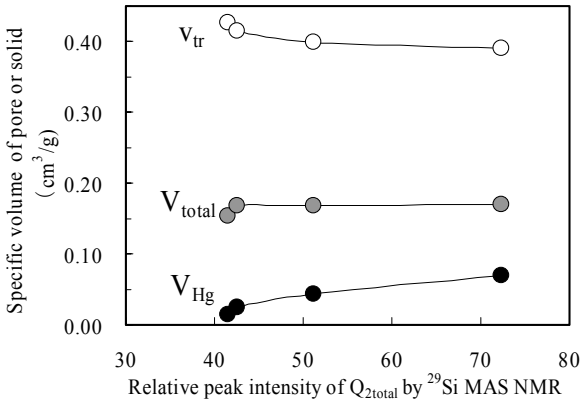

Fig. 18 Relationship between pore volumes and Q_{2total}.

(6) Specific surface area measured with BET-N_2 and ESW S2-H_2O decreased significantly with an increase in

polymerization of silicate anions in C-S-H, implying that the drying was responsible to the polymerization and the development of cohesive structures of C-S-H.

(7) The drying-induced pore coarsening of HCP, as measured with MIP, was attributed to the formation of cohesive structures resulting from the polymerization of silicate anion chains in C-S-H.

References

Adolphs, J. and Setzer, M. J. (1996a). "A model to describe adsorption isotherms." *J. Colloid and Interface Science.*, 180, 70-76.

Adolphs, J. and Setzer, M. J. (1996b). "Energetic classification of adsorption isotherms." *J. Colloid and Interface Science.*, 184, 443-448.

Adolphs, J. and Setzer, M. J. (1998). "Description of gas adsorption isotherms on porous and dispersed systems with the excess surface work model." *J. Colloid and Interface Science.*, 207, 349-354.

Aligizaki, K. K. (2006). "Pore structure of cement-based materials, testing, interpretation and requirements." London and New York, Taylor & Francis.

Bentur, A., Berger, R. L., Lawrence, Jr. F. V., Milestone, N. B., Mindess, S. and Young, J. F. (1979). "Creep and drying shrinkage of calcium silicate pastes: III, A hypothesis of irreversible strains." *Cement and Concrete Research*, 9, 83-96.

Birchall, J. D. and Thomas. N. L. (1984). "The mechanism of retardation of setting of OPC by sugars." *Proc. Br. Ceram. Soc.*, 35, 305-315.

Brough, A. R., Groves, G. W., Richardson, I. G., Rodger, S. A. and Dobson, C. M. (1994). "Kinetics of hydration and other reactions of calcium silicates and cements." *Application of NMR Spectroscopy to Cement Science*, Gordon and Breach Science Publishers, 201-211.

Brunauer, S., Emmett, P. H. and Teller, E. (1938). "Adsorption of gases in multimolecular layers." *Journal of the American Chemical Society*, 60(2), 309-319.

Brunauer, S. and Greenberg, S. A. (1962). "The hydration of tricalcium silicate and β-Dicalcium silicate at room temperature." *4th International Symposium on the Chemistry of Cement*, 1, 135-163,

Daimon, M., Abo-El-Enein, S., Hosaka, G., Goto, S. and Kondo, R. (1977). "Pore structure of calcium silicate hydrate in hydrated tricalcium silicate." *Journal of The American Ceramic Society*, 60(3-4), 110-114.

Diamond, S. (2000). "Mercury porosimetry: An inappropriate method for the measurement of pore size distributions in cement-based materials." *Cement and Concrete Research*, 30(10), 1517-1525.

Dollimore, D. and Heal, G. R. (1964). "An improved method for the calculation of pore size distribution from adsorption data." J. Appl. Chem., 14, 109-114.

Feldman, R. F. and Serada, P. J. (1968). "A model for hydrated Portland cement paste as deduced from sorption-length change and mechanical properties." *Materials and Structures*, 1(6), 50-520.

Galle, C. (2001). "Effect of drying on cement-based materials pore structure as identified by mercury intrusion porosimetry A comparative study between oven-, vacuum-, and freeze-drying." *Cement and Concrete Research*, 31(10), 1467-1477

Grimmer, A-R. (1994). "Structural investigation of calcium silicates from 29Si chemical shift measurements." *Application of NMR spectroscopy to cement science*, Gordon and Breach Science Publishers, 113-151.

Hironaga, M. and Sekiguchi, A. (1999). "The chemical change of calcium silicate hydrates on the high temperature." *Proceedings of Annual Conference of The Japan Society Of Civil Engineers*, 54, 70-71

Jennings, H. M. (2000). "A model for the microstructure of calcium silicate hydrate in cement paste." *Cement and Concrete Research*, 30, 101-116.

Jennings, H. M. (2004). "Colloid model of C-S-H and implications to the problem of creep and shrinkage." *Material and Structures / Concrete Science and Engineering*, 37, 59-70.

Jennings, H. M. and Thomas, J. J. (2004). "A discussion of the paper "The BET-specific surface area of hydrated Portland cement and related materials" by Ivan Odler." *Cement and Concrete Research*, 34, 1959-1960.

Klur, I., Pollet, B., Virlet, J. and Nonat, A. (1998). "C-S-H structure evolution with calcium content by multinuclear NMR." *Nuclear Magnetic Resonance Spectroscopy of Cement-Based Materials*, Springer, 119-141.

McClellan, A. L. and Harnsberger, H. F. (1967). "Cross-sectional areas of molecules adsorbed on solid surfaces." *Journal of Colloid and Interface Science*, 23, 577-599.

Milestone, N. B. (1980). "Ageing and drying of tricalcium silicate pastes." *Proceedings of the 7th International congress on the chemistry of cement*, 3, Paris, VI-61-66.

Moukwa, M. and Aitcin, P.-C. (1988). "The effect of drying on cement pastes pore structure as determined by mercury prosimetry." *Cement and Concrete Research*, 18(5), 745-752.

Odler, I. (2003). "The BET-specific surface area of hydrated Portland cement and related materials." *Cement and Concrete Research*, 33, 2049–2056.

Parrott, L. J. and Young, J. F. (1981). "Effect of prolonged drying upon the silicate structure of hydrated alite pastes." *Cement and Concrete Research*, 11, 11-17.

Parry-Jones, G., Al-Tayyib, A. J., Al-Dulaijan, S. U. and Al-Mana, A. I. (1989). "29Si MAS-NMR hydration and compressive strength study in cement paste." *Cement and Concrete Research*, 19, 228-234.

Powers, T. C. and Brownyard, T. L. (1947). "Studies of physical properties of hardened portland cement paste." *Bulletin No.22, Res. Lab. of Portland Cement*

Association, Skokie, IL, U.S.A., reprinted from J. Am. Concr. Inst. (Proc.), 43, 101-132, 249-336, 469-505, 549-602, 669-712, 845-880, 933-992.

Tanaka, K., Hashida, H. and Hashi, N. (1994). "Pore structure and moisture of mortar at early ages during drying." *J. Struct. Constr. Eng.*, AIJ, 460, 11-18. (in Japanese)

Thomas, J. and Jennings, H. M. (2006). "A colloidal interpretation of chemical aging of the C-S-H gel and its effects on the properties of cement paste." *Cement and Concrete Research*, 36, 30–38.

Uchikawa, H., Uchida, S. and Mihara, Y. (1980). "*Review of the 34th General Meeting The Cement Association of Japan*." 34, 58-62.

Uchikawa, H., Hanehara, S. and Sawaki, D. (1991). "Structural change of hardened mortar by drying." *3rd NCB international seminar (New Dehli-India)*, 4, VIII-1-VIII-12.

Washburn, E. W. (1921). "Note on a method of determining the distribution of pore sizes in a porous material." *Proceedings of the National Academy of Sciences*, 7(4), 115-116.